Available online at www.sciencedirect.com
SCIENCE DIRECT®
Comput. Methods Appl. Mech. Engrg. 195 (2006) 1946–1957
Computer methods in applied mechanics and engineering
www.elsevier.com/locate/cma

p-Version FEM for structural acoustics with a posteriori error estimation ☆

S. Dey [a,*], D.K. Datta [a], J.J. Shirron [b], M.S. Shephard [c]

[a] *SFA Inc./Naval Research Laboratory, Washington, DC 20375, United States*
[b] *Metron Inc., Reston, VA 20190, United States*
[c] *SCOREC, Rensselaer Polytechnic Institute, Troy, NY 12180, United States*

Received 1 April 2004; received in revised form 2 November 2004; accepted 4 November 2004

Abstract

We demonstrate the advantages of using *p*-version finite element approximations for structural-acoustics problems in the mid-to-high frequency regime. We then present a sub-domain-based a posteriori error estimation procedure to quantify the errors in the setting of a 3D interior-acoustics problem with resonances, and give numerical results. Effectivity indices show robust behavior of the error estimator away from the resonant frequencies.

Keywords: Fluid–structure interaction; *p*-Version FEM; Sub-domain error estimation; Effectivity indices

1. Introduction

Finite elements discretizations using high polynomial degrees, the so-called *p*-version finite element method (FEM), are particularly well-suited for accurate solutions of structural acoustics, elastodynamics and wave-related problems at mid to high frequencies. Both theory [1] and numerical experiments [4] show that, for smooth problems, they offer superior rates of error convergence compared to low-order (*h*-version) discretizations due to better control of the dispersion error [5,6]. Consider, for example, the problem of computing the pressure distribution inside a fuselage-like volume (Fig. 1) for given Neumann data on the bounding cylindrical surface which is smooth. We evaluate uniform *p*-refinement on the depicted mesh

☆ This research was funded by NASA and HPCMPO under the CHSSI initiative.
* Corresponding author. Address: SFA Inc./NRL, 2200 Defense Highway, Suite 405, Crofton, MD 21114, USA. Tel.: +1 202 767 7321; fax: +1 202 404 7420.
E-mail address: dey@pa.nrl.navy.mil (S. Dey).

0045-7825/$ - see front matter © 2005 Published by Elsevier B.V.
doi:10.1016/j.cma.2004.11.030

and also evaluate uniform h-refinement starting from the same mesh using $p = 1$. Fig. 2 shows the exponential convergence rate for uniform p refinement compared to only an algebraic rate for uniform h refinement. We also obtain similar convergence rates in the context of three-dimensional elastodynamics. We demonstrate this by computing the non-zero natural frequencies of a block of steel with *Young*'*s* modulus $2.07e^{11}$ and *Poisson*'*s* ratio 0.3. The dimensions of the block are $0.461\ \text{m} \times 0.461\ \text{m} \times 0.152\ \text{m}$. For p-refinement we use one hexahedral element for the entire domain. h-refinement uses uniform sub-division of this single element. Fig. 3 shows the convergence of error versus solution time for the fourth non-zero natural frequency of a block of steel as compared to experimental data [8]. Once again, for a given target error p-refinement requires less computing time than h-refinement. These trends also carry over to problems of fluid–structure interaction. Ref. [7] evaluates various p-refinement schemes for problems of interior and exterior elasto-acoustics with a range of acoustic and mechanical excitations. Results we present later also demonstrate exponential convergence for coupled elasto-acoustics. It must be noted that for problems where the solution has singularities, carefully designed hp-approximations are needed to preserve exponential convergence.

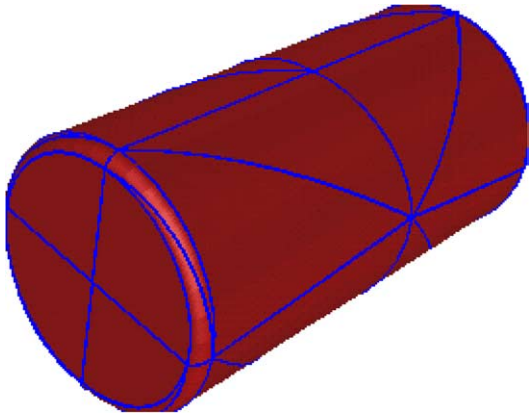

Fig. 1. Domain and the coarsest mesh considered for interior noise problem.

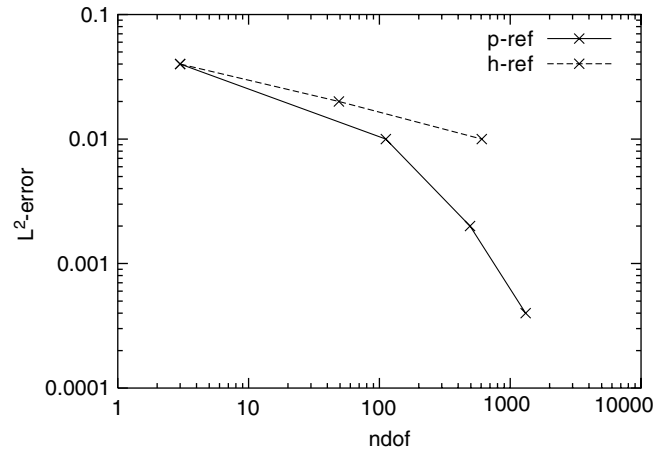

Fig. 2. Convergence of L^2-norm of error in pressure for interior noise problem.

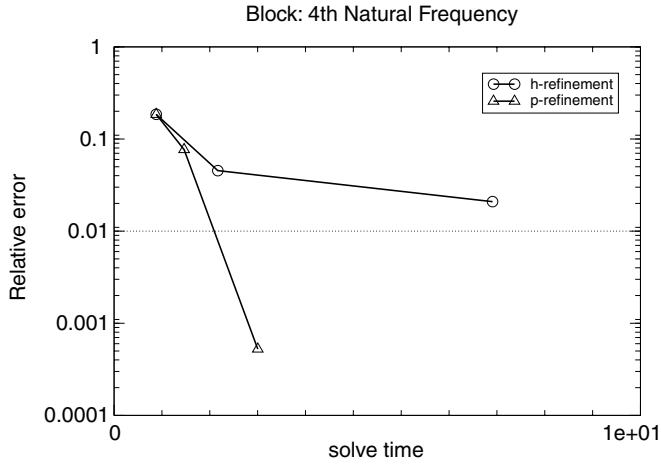

Fig. 3. Error in computing natural frequency as a function of CPU time for *h*- and *p*-refinements.

With the increasing role of finite element-based numerical simulations in large-scale engineering design and analysis, a substantial effort is being focused on validation and verification of various techniques [2]. Validation aims to ensure the appropriateness of the mathematical model for the physical system being simulated. This is typically achieved by comparing the simulation results against experimental data. Verification ensures the correctness of the approximate numerical solution of a selected mathematical model. A central aspect of verification involves estimation and effective control of model discretization errors in numerical simulations. Effective a posteriori estimation of the errors not only increases the reliability of the computed solution, but is also the first step toward controlling it in an adaptive manner.

In this paper we present an a posteriori error estimation technique based on the sub-domain residual for *p*-version finite element solutions of coupled elasto-acoustic problems in three spatial dimensions. Residual-based implicit error estimators have been found to be more robust than other types of error estimators (see [9]). Residual-based error estimators require the solution of local problems on an element (or patch of elements) with either Neumann or Dirichlet boundary conditions. For Neumann boundary conditions, an equilibrated flux is imposed on the boundary. Though this can lead to very good error estimation, this method is expensive and cumbersome. This is especially true for meshes in 3D with topologically mixed elements (i.e., meshes with combinations of tetrahedrons, wedges, hexahedrons, etc.) and, therefore, it is seldom used in practice. Various versions of sub-domain-based error estimation remove the complicated construction of equilibrated fluxes on the patch boundaries (see [10–12]). In this paper we consider one method with Dirichlet boundary condition on the local sub-domain boundaries. The local sub-domains are constructed based on the elements connected to the mesh vertices. We give numerical results by computing the so-called *effectivity* indices, i.e., the ratio of the estimated error to the exact error (see [9]), to show the robustness of the procedures for frequency-dependent problems and *p*-refinement.

The rest of the paper is organized as follows. In Section 2 we outline the physical and mathematical description of our model problem and review the basics of a finite element-based discretization of the problem and parameters that control the numerical error. In Section 3 we give the formulation of the residual equation and the sub-domain residual error estimator for 3D structural acoustics. We present numerical experiments in Section 4 that show the effectivity indices of the estimated error as a function of both the wave number and the maximum polynomial degree of the finite element discretization. We conclude with a discussion of the results and open issues in Section 5.

2. Structural-acoustics overview

We are concerned with computing the response of a coupled fluid-elastic system subjected to mechanical and/or acoustical excitation. The problem domain typically involves a (partially) fluid-filled elastic shell-like structure as shown in Fig. 4. If the structure is itself embedded in another infinite fluid then it is known as the *exterior* problem. If there is no fluid exterior to the structure then it is an *interior* problem. In this paper we focus on interior problems.

2.1. Model problem

The geometric description of a typical interior problem is depicted in Fig. 4(a). It consists of a uniform, isotropic, hollow elastic shell filled with a fluid. The corresponding computational model is shown in Fig. 4(b), where Ω^{s} denotes the structural domain, Ω^{f} denotes the fluid domain, $\Gamma^{\mathrm{int}} = \overline{\Omega}^{\mathrm{f}} \cap \overline{\Omega}^{\mathrm{s}}$ denotes the interior boundary of the structure, Γ^{ext} denotes the exterior boundary of the structure, and n^{int} and n^{ext} are unit vectors normal to the corresponding surface.

The governing partial differential equations for a pressure-displacement formulation [3] in Cartesian coordinates are

$$\sigma_{jk,k} + \rho_{\mathrm{s}}\omega^2 u_j = 0 \quad \text{in } \Omega^{\mathrm{s}}, \tag{1}$$

$$\Delta\phi + k^2\phi = 0 \quad \text{in } \Omega^{\mathrm{f}}, \tag{2}$$

where ϕ is the fluid pressure field, u_j are the components of the elastic displacement field $\mathbf{u}$, ω is the circular frequency of excitation and ρ_{s} is the density of the shell. The acoustic wave number is $k = \omega/c$, where c is the speed of sound in the fluid. The components of the stress tensor are given by

$$\sigma_{jk}(\mathbf{u}) = \lambda\delta_{jk}\epsilon_{kk}(\mathbf{u}) + 2\mu\epsilon_{jk}(\mathbf{u}),$$

where λ, μ are the Lamé parameters, and $\epsilon_{kj}(\mathbf{u}) = \frac{1}{2}(u_{j,k} + u_{k,j})$ are the components of the symmetric strain tensor. We denote by $\mathbf{t}^{\mathrm{ext}}$ the traction applied to Γ^{ext}. We shall assume that no independently known elastic traction is applied to the fluid/structure interface Γ^{int}. The boundary conditions are then

$$\sigma_{jk}n_k^{\mathrm{ext}} = t_j^{\mathrm{ext}} \quad \text{on } \Gamma^{\mathrm{ext}}, \tag{3}$$

$$\sigma_{jk}n_k^{\mathrm{int}} = \phi n_k^{\mathrm{int}} \quad \text{on } \Gamma^{\mathrm{int}}, \tag{4}$$

$$\frac{\partial\phi}{\partial n^{\mathrm{int}}} = \rho_{\mathrm{f}}\omega^2 u_j n_j^{\mathrm{int}} \quad \text{on } \Gamma^{\mathrm{int}}, \tag{5}$$

where ρ_{f} is the fluid density.

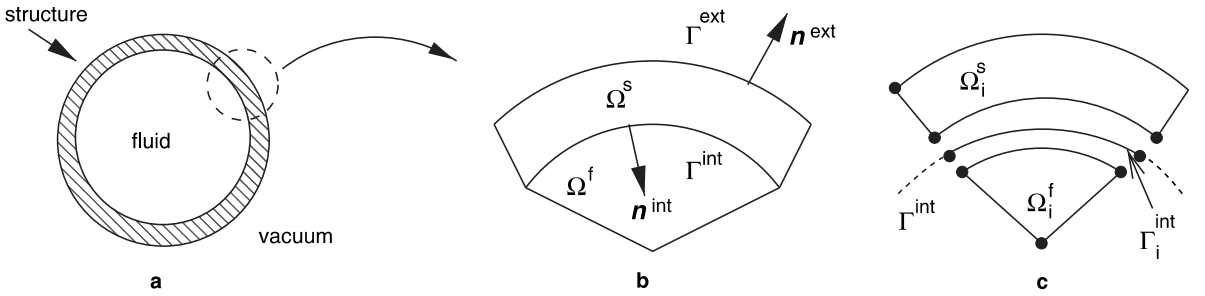

Fig. 4. Model problem: (a) physical domain, (b) computational domain and (c) finite element discretization.

Following standard Galerkin techniques we can state a weak (variational) form of the problem as: Find an elastic displacement field $\mathbf{u} = (u_1,u_2,u_3)$ with $u_j \in H^1(\Omega^s)$ and acoustic pressure field $\phi \in H^1(\Omega^f)$ such that

$$\mathscr{B}_{11}(\mathbf{u},\mathbf{v}) + \mathscr{B}_{12}(\phi,\mathbf{v}) = \mathscr{L}(\mathbf{v}), \tag{6}$$

$$\mathscr{B}_{21}(\mathbf{u},\psi) + \mathscr{B}_{22}(\phi,\psi) = 0, \tag{7}$$

for all $v_j \in H^1(\Omega^s)$ (components of vector $\mathbf{v}$) and $\psi \in H^1(\Omega^f)$ where

$$\mathscr{B}_{11}(\mathbf{u},\mathbf{v}) = \int_{\Omega_s} (\sigma_{jk}(\mathbf{v})\epsilon_{jk}(\mathbf{u}) - \rho_s\omega^2\mathbf{v}\cdot\mathbf{u})\,\mathrm{d}\Omega, \tag{8}$$

$$\mathscr{B}_{12}(\phi,\mathbf{v}) = \int_{\Gamma_{\mathrm{int}}} \phi\mathbf{v}\cdot\mathbf{n}^{\mathrm{int}}\,\mathrm{d}\Gamma, \tag{9}$$

$$\mathscr{B}_{21}(\mathbf{u},\psi) = \rho_f\omega^2 \int_{\Gamma_{\mathrm{int}}} \psi\mathbf{u}\cdot\mathbf{n}^{\mathrm{int}}\,\mathrm{d}\Gamma, \tag{10}$$

$$\mathscr{B}_{22}(\phi,\psi) = \int_{\Omega} (\nabla\phi\cdot\nabla\psi - k^2\phi\psi)\,\mathrm{d}\Omega, \tag{11}$$

$$\mathscr{L}(\mathbf{v}) = \int_{\Gamma^{\mathrm{ext}}} \mathbf{v}\cdot\mathbf{t}^{\mathrm{ext}}\,\mathrm{d}\Gamma. \tag{12}$$

For more details refer to [4].

Let $\Delta_h^s(\Delta_h^f)$ be the spatial discretization of the solid (fluid) domain $\Omega^s(\Omega^f)$, with h representing a measure of the spatial mesh size. We will assume h to be fixed. Let $p_f \geqslant 1$ and $p_s \geqslant 1$ be polynomial degrees of approximation over finite elements in the fluid and solid domains, respectively. We denote by $\mathscr{U}^{hp_f}(\Omega^f)$ $(\mathscr{U}^{hp_s}(\Omega^s))$ the (finite-dimensional) space of all continuous piecewise polynomial functions of degree at most $p_f(p_s)$ on each element in $\Omega^f(\Omega^s)$. Our problem is then to find displacement components $u_j^{hp_s} \in \mathscr{U}^{hp_s}(\Omega^s) \subset H^1(\Omega^s)$ and pressure $\phi^{hp_f} \in \mathscr{U}^{hp_f}(\Omega^f) \subset H^1(\Omega^f)$ such that

$$\mathscr{B}_{11}(\mathbf{u},\mathbf{v}) + \mathscr{B}_{12}(\phi,\mathbf{v}) = \mathscr{L}(\mathbf{v}), \tag{13}$$

$$\mathscr{B}_{21}(\mathbf{u},\psi) + \mathscr{B}_{22}(\phi,\psi) = 0, \tag{14}$$

for all $v_j \in \mathscr{U}^{hp_s}(\Omega^s)$ and $\psi \in \mathscr{U}^{hp_f}(\Omega^f)$.

3. A posteriori error estimation

In this section we outline the formulation of the residual equation and then derive a sub-domain residual estimator for 3D interior structural acoustics problems.

3.1. The residual equation

Let

$$\mathbf{e} = \mathbf{u} - \mathbf{u}^{hp_s} \tag{15}$$

and

$$\epsilon = \phi - \phi^{hp_f} \tag{16}$$

denote the errors in finite element approximations $\mathbf{u}^{hp_s}$ and ϕ^{hp_f}, respectively. On substituting $\mathbf{u} = \mathbf{u}^{hp_s} + \mathbf{e}$, and $\phi = \phi^{hp_f} + \epsilon$ into (6) and (7) we see that the error satisfies

$$\mathscr{B}_{11}(\mathbf{e},\mathbf{v}) + \mathscr{B}_{12}(\epsilon,\mathbf{v}) = \mathscr{L}(\mathbf{v}) - \mathscr{B}_{11}(\mathbf{u}^{hp_s},\mathbf{v}) - \mathscr{B}_{12}(\phi^{hp_f},\mathbf{v}), \tag{17}$$

$$\mathscr{B}_{21}(\mathbf{e},\psi) + \mathscr{B}_{22}(\epsilon,\psi) = -\mathscr{B}_{21}(\mathbf{u}^{hp_s},\psi) - \mathscr{B}_{22}(\phi^{hp_f},\psi), \tag{18}$$

for all $v_j \in H^1(\Omega^s)$ and $\psi \in H^1(\Omega^f)$. We could approximate the error by introducing enriched (higher-dimensional) spaces $\mathscr{U}^{hp'_s}(\Omega^s)$ and $\mathscr{U}^{hp'_f}(\Omega^f)$ for polynomial degrees $p'_s > p_s$ and $p'_f > p_f$, then solving the problem:

Find $e_j^{hp'_s} \in \mathscr{U}^{hp'_s}(\Omega^s)$ and $\epsilon^{hp'_f} \in \mathscr{U}^{hp'_f}(\Omega^f)$ such that (17) and (18) is satisfied for all $v_j \in \mathscr{U}^{hp'_s}(\Omega^s)$ and $\psi \in \mathscr{U}^{hp'_f}(\Omega^f)$.

An estimate of the error obtained in this way would have the best possible *effectivity index*. However this approach is very computationally expensive and, hence, impractical. Nevertheless, this approach provides a very good way to check the implementation of the residual calculation since the estimated error converges to the exact error as $p'_s \to \infty$ and $p'_f \to \infty$. This estimator will be referred to as the *global residual estimator*. The estimated error in the L^2-norm is then obtained by

$$\mathscr{E}^{\mathrm{GRE}}_{\mathbf{u},L^2(\Omega^s)} \stackrel{\mathrm{def}}{=} \sqrt{\sum_{\tau\in\Delta_h^s} \|\mathbf{e}^{hp'_s}\|^2_{L^2(\tau)}} \tag{19}$$

and

$$\mathscr{E}^{\mathrm{GRE}}_{\phi,L^2(\Omega^f)} \stackrel{\mathrm{def}}{=} \sqrt{\sum_{\tau\in\Delta_h^f} \|\epsilon^{hp'_f}\|^2_{L^2(\tau)}}, \tag{20}$$

where τ is a finite element in the solid (fluid) domain.

3.2. The sub-domain residual estimator

The global residual estimator in the previous section requires us to solve the original problem twice, once with the approximation spaces $\mathscr{U}^{hp_s}(\Omega^s)$ and $\mathscr{U}^{hp_f}(\Omega^f)$, then again with the enriched spaces $\mathscr{U}^{hp'_s}(\Omega^s)$ and $\mathscr{U}^{hp'_f}(\Omega^f)$. This procedure is not computationally efficient, so it would be desirable to obtain an error estimator that required us to solve only local problems. Here we present the technique known as the sub-domain residual estimator based on the solution of the residual equation on local sub-domains with Dirichlet boundary conditions. The sub-domains are created based on elements connected to the mesh vertices.

Let φ_X be the piecewise-linear basis function corresponding to a vertex X. Let $\varpi_X^s(\varpi_X^f)$ denote the intersection of the support of φ_X with the domain $\Omega^s(\Omega^f)$, which is the union of all solid (fluid) elements connected to vertex X, i.e.,

$$\varpi_X^{s,f} = \mathrm{supp}(\varphi_X) \cap \Omega^{s,f} = \bigcup_{\substack{\tau\in\Delta_h^{s,f}\\ X\in\partial\tau}} \tau. \tag{21}$$

We will refer to $\varpi_X^s(\varpi_X^f)$ as the solid (fluid) sub-domain centered on vertex X. Let us introduce the approximation spaces

$$\mathscr{U}_0^{hp'_{s,f}}(\varpi_X^{s,f}) \stackrel{\mathrm{def}}{=} \left\{ v \in \mathscr{U}^{hp'_{s,f}}(\varpi_X^{s,f}) | v|_{\partial\varpi_{X,D}^{s,f}} = 0 \right\}, \tag{22}$$

where $p'_s > p_s$, $p'_f > p_f$ and

$$\partial\varpi_{X,D}^{s,f} \stackrel{\mathrm{def}}{=} \partial\varpi_X^{s,f} \setminus \Gamma^{\mathrm{int}} \setminus \Gamma^{\mathrm{ext}}. \tag{23}$$

Then we pose the sub-domain residual problem: Find $\hat{e}_j \in \mathscr{U}_0^{hp'_s}(\varpi_X^s)$ and $\hat{\epsilon} \in \mathscr{U}_0^{hp'_f}(\varpi_X^f)$ such that

$$\mathscr{B}_{11}(\hat{\mathbf{e}},\mathbf{v}) + \mathscr{B}_{12}(\hat{\epsilon},\mathbf{v}) = \mathscr{L}(\mathbf{v}) - \mathscr{B}_{11}(\mathbf{u}^{hp_s},v_j) - \mathscr{B}_{12}(\phi^{hp_f},v_j), \tag{24}$$

$$\mathscr{B}_{21}(\hat{\mathbf{e}},\psi) + \mathscr{B}_{22}(\hat{\epsilon},\psi) = -\mathscr{B}_{21}(\mathbf{u}^{hp_s},\psi) - \mathscr{B}_{22}(\phi^{hp_f},\psi), \tag{25}$$

for all $v_j \in \mathscr{U}_0^{hp'_s}(\varpi_X)$ and $\psi \in \mathscr{U}_0^{hp'_f}(\varpi_X^f)$.

Note that when $X \in \Omega^{\mathrm{s}}$ we take $\hat{\epsilon} = 0$ and ignore (25), for $X \in \Omega^{\mathrm{f}}$ we take $\hat{\mathbf{e}} = 0$ and ignore (24), while for $X \in \Gamma^{\mathrm{int}}$ we solve a coupled problem by considering both (24) and (25).

The estimated error in the L^2-norm is then obtained by

$$\mathscr{E}^{\mathrm{SDR}}_{\mathbf{u},L^2(\Omega_{\mathrm{s}})} \stackrel{\mathrm{def}}{=} \sqrt{\sum_X \sum_{\tau \in \varpi^{\mathrm{s}}_X} \|\hat{\mathbf{e}}\|^2_{L^2(\tau)}} \tag{26}$$

and

$$\mathscr{E}^{\mathrm{SDR}}_{\phi,L^2(\Omega_{\mathrm{f}})} \stackrel{\mathrm{def}}{=} \sqrt{\sum_X \sum_{\tau \in \varpi^{\mathrm{f}}_X} \|\hat{\epsilon}\|^2_{L^2(\tau)}}. \tag{27}$$

4. Numerical results and discussion

4.1. Model problem and reference solution

To verify the error estimators themselves, we consider the problem of a fluid-filled spherical shell subjected to a uniform time-harmonic normal traction applied to the outer surface. Since the traction is independent of the polar and azimuthal angles (θ, ϕ), the interior pressure is a function only of the radial coordinate r, i.e.,

$$\phi(r, \theta, \phi) = A j_0(kr), \tag{28}$$

where j_0 is the spherical Bessel function of the first kind of order zero. Due to spherical symmetry the angular components of the displacement field vanish ($u_\theta = u_\phi = 0$) and the radial displacement u_r is a function only of r. Consequently, (1) reduces to a second-order ordinary differential equation whose solution can be computed via a spectral finite-element method. We have computed the reference solution based on interpolating u_r with Legendre polynomials of degree 6. It is known [3] that the frequency-domain solution of this problem has resonances in both the interior pressure and radial displacement.

Fig. 5(a) and (b) plot the L^2-norm of the pressure ϕ and the L^2-norm of the radial displacement u_r, respectively, for $ka = 1, \ldots, 15$. Here the Eqs. (1)–(5) were considered on a spherical shell of unit radius with the input data: $\mathbf{t}^{\mathrm{ext}} = \mathbf{n}^{\mathrm{ext}}\ \mathrm{Nm}^{-2}$, $c = 320\ \mathrm{ms}^{-1}$, $\rho_{\mathrm{s}} = 7800\ \mathrm{kg\,m}^{-3}$, $\rho_{\mathrm{f}} = 1.25\ \mathrm{kg\,m}^{-3}$, Young's modulus

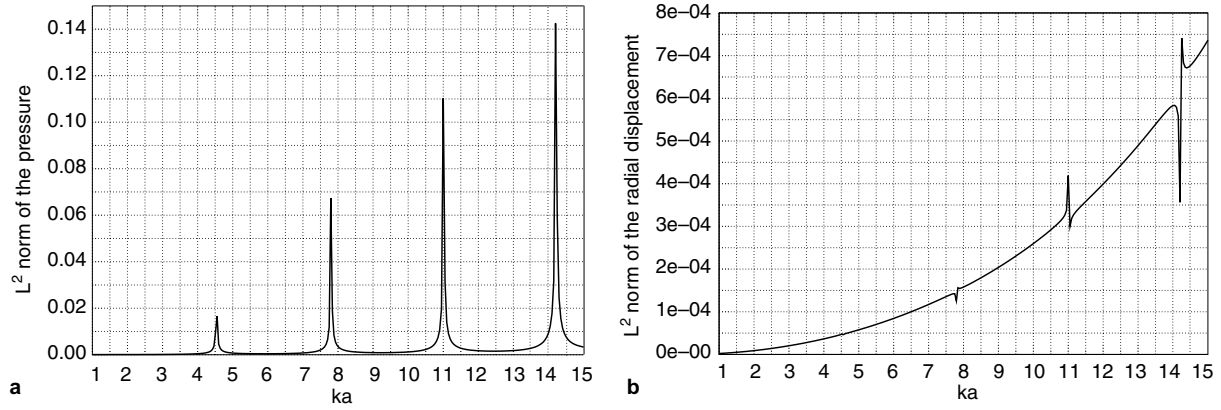

Fig. 5. Resonance in frequency response for model problem: (a) interior pressure and (b) radial displacement.

$E = 2.0 \times 10^{11}$ Nm^{-2}, and Poisson's ratio $v = 0.3$. We note the resonant peaks around $k \approx 4.5$, 8, 11, 14 as shown in Fig. 5.

Fig. 6 depicts one quarter of a slice of the volume mesh used in the numerical computations presented here. Note that the domain was discretized using 3D finite elements consisting of hexahedrons, and wedges.

Tables 1 and 2 give the relative errors for the pressure and the radial displacement, respectively, in the L^2-norm. Fig. 7 plots the convergence of the exact error for uniform p-refinement. As expected for a smooth problem, we see exponential nature of convergence.

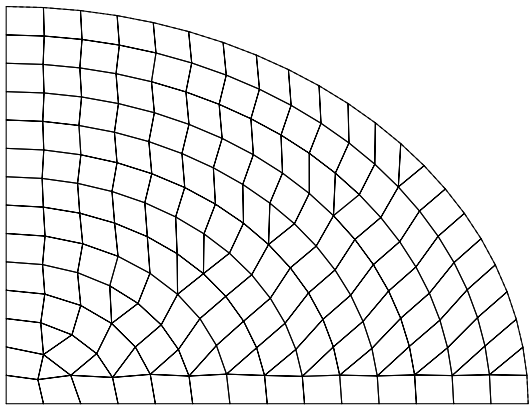

Fig. 6. Quarter of the 3D fluid-mesh sliced at $\phi = 0$. A single conformal-layer of elastic elements terminates the bounded fluid-volume.

Table 1
Relative error in pressure, $\|\phi - \phi^{hp_f}\|_{L^2(\Omega_f)}/\|\phi\|_{L^2(\Omega_f)}$: here $p_s = p_f$

ka	$p_f = 2$	$p_f = 3$	ka	$p_f = 2$	$p_f = 3$
1	7.446e−04	1.37093e−04	9	6.173e−03	3.275e−03
2	1.031e−03	3.44390e−04	10	1.368e−02	3.278e−03
3	4.499e−03	1.19852e−03	11	1.607e−01	5.617e−02
4	1.589e−03	8.58965e−04	12	1.835e−02	5.442e−03
5	1.206e−03	8.92646e−04	13	9.268e−03	6.673e−03
6	1.941e−03	1.43849e−03	14	4.691e−02	5.113e−02
7	4.290e−03	3.00484e−03	15	1.586e−02	1.057e−02
8	7.098e−03	9.92800e−03			

Table 2
Relative error in the radial displacement $\|u_r - u_r^{hp_s}\|_{L^2(\Omega_s)}/\|u_r\|_{L^2(\Omega_s)}$: here $p_f = p_s$

ka	$p_s = 2$	$p_s = 3$	ka	$p_s = 2$	$p_s = 3$
1	2.008e−03	4.171e−04	9	4.269e−03	2.170e−03
2	2.029e−03	4.196e−04	10	5.862e−03	2.956e−03
3	2.076e−03	4.266e−04	11	7.174e−02	7.232e−02
4	2.281e−03	6.171e−04	12	1.852e−02	5.676e−03
5	2.161e−03	1.275e−03	13	7.208e−03	5.858e−03
6	2.225e−03	1.080e−03	14	4.649e−02	4.751e−02
7	2.750e−03	2.095e−03	15	1.172e−02	9.823e−03
8	8.502e−03	7.420e−03			

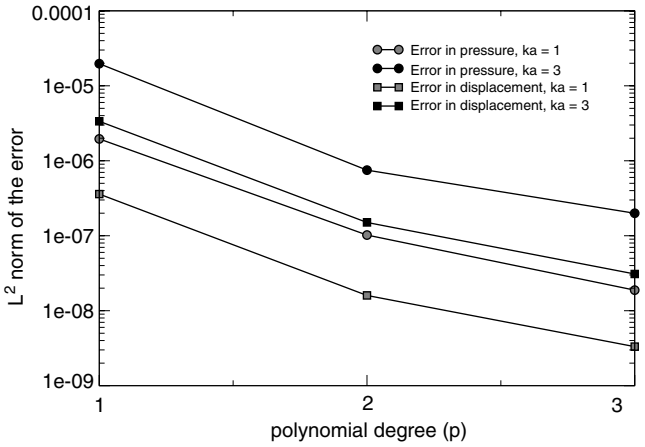

Fig. 7. Exact error convergence for uniform p-refinement for model problem.

4.2. Performance of the estimators

To evaluate the performance of the error estimators we computed the effectivity indices of the estimated error, in the L^2-norm, in the pressure and the radial displacement u_r for a range of frequencies and p-approximations. The effectivity index of the estimated error in the pressure in L^2-norm is defined as

$$\eta^{\mathrm{EST}}_{\phi,L^2(\Omega_{\mathrm{f}})} = \mathscr{E}^{\mathrm{EST}}_{\phi,L^2(\Omega_{\mathrm{f}})} / \|\phi - \phi^{hp_{\mathrm{f}}}\|_{L^2(\Omega_{\mathrm{f}})} \tag{29}$$

and the effectivity index of the estimated error in the radial displacement in L^2-norm is defined as

$$\eta^{\mathrm{EST}}_{u_r,L^2(\Omega_{\mathrm{s}})} = \mathscr{E}^{\mathrm{EST}}_{u_r,L^2(\Omega_{\mathrm{s}})} / \|u_r - u_r^{(hp_{\mathrm{s}})}\|_{L^2(\Omega_{\mathrm{s}})} \tag{30}$$

with EST = GRE, SDR. The exact solutions ϕ, and u_r were computed as discussed in Section 4.1.

Table 3 gives the effectivity indices of the estimated error in the pressure in L^2-norm ($\eta^{\mathrm{GRE}}_{\phi,L^2(\Omega_{\mathrm{f}})}$) for $p_{\mathrm{f}} = 2$ and the error in the radial displacement ($\eta^{\mathrm{GRE}}_{u_r,L^2(\Omega_{\mathrm{f}})}$) for $p_{\mathrm{s}} = 2$ using the global residual estimator for $ka = 1,\ldots,15$. Here we used $p'_{\mathrm{f}} = 3$, and $p'_{\mathrm{s}} = 3$. The numbers given in italics indicate the effectivity indices near the resonant frequencies. Note that the estimator has good effectivity indices except near the resonant frequencies as expected. If not computationally prohibitive, as mentioned earlier, this estimator can provide

Table 3
Effectivity indices $\eta^{\mathrm{GRE}}_{\phi,L^2(\Omega_{\mathrm{f}})}$ (for pressure) and $\eta^{\mathrm{GRE}}_{u_r,L^2(\Omega_{\mathrm{f}})}$ (for radial displacement) using the global residual estimator with $p_{\mathrm{f}} = p_{\mathrm{s}} = 2$ and $p'_{\mathrm{f}} = p'_{\mathrm{s}} = 3$

ka	Pressure	Radial displacement	ka	Pressure	Radial displacement
1	0.8377	0.9968	9	1.0418	0.6853
2	0.8030	0.9922	10	0.9242	0.6813
3	0.7721	0.9795	*11*	*0.6510*	*0.1413*
4	0.9163	0.9045	12	0.8200	0.8053
5	0.6518	0.9786	13	1.1207	0.6371
6	0.8590	0.9842	*14*	*1.9303*	*0.0730*
7	0.9302	0.8418	15	1.1247	0.4155
8	*0.5115*	*0.2937*			

Numbers in italics indicate ka is near a resonant frequency.

very robust measure of the error. The relative additional amount of computational cost for this estimator is 1.3–1.5 while for the sub-domain residual is around 0.1–0.3 for the examples considered here.

Tables 4 and 5 give the effectivity indices of the estimated error in the pressure in L^2-norm ($\eta^{\mathrm{SDR}}_{\phi,L^2(\Omega_{\mathrm{f}})}$) for $p_{\mathrm{f}} = 2,3$, and estimated error in the radial displacement in L^2-norm ($\eta^{\mathrm{SDR}}_{u_r,L^2(\Omega_{\mathrm{f}})}$) for $p_{\mathrm{s}} = 2,3$, respectively, using the sub-domain residual estimator for $ka = 1,\ldots,15$. Here we used $p'_{\mathrm{f}} = p_{\mathrm{f}} + 2$, and $p'_{\mathrm{s}} = p_{\mathrm{s}} + 2$. The numbers given in italics indicate the effectivity indices near the resonant frequencies. For the pressure we get good effectivity indices except near the resonant frequencies, however for the displacement we get low effectivity indices for $ka > 8$. As ka increases we note that the resonant frequencies occur more frequently and the gap between two resonant frequency gets smaller. This causes the effectivity indices to deteriorate since the entire band of frequency is close to the resonant frequency.

Remark 1. For the case of $ka = 4$, and $p_{\mathrm{f}} = 2$ ($p_{\mathrm{s}} = 2$) we computed the local elementwise effectivity indices. For the fluid (solid) elements along the fluid-solid interface, Γ^{int} the effectivity indices are in the range of 0.2–1.5 (0.4–2.0), while for the elements which are completely embedded in the fluid domain the effectivity indices are in the range of 0.2–5.0. The higher effectivity indices are mostly for those elements which have relatively low local error. Note that for this example problem all the solid elements are touching Γ^{int}.

Table 4
Effectivity indices of the estimated error in the pressure in L^2-norm ($\eta^{\mathrm{SDR}}_{\phi,L^2(\Omega_{\mathrm{f}})}$) for $p_{\mathrm{s}} = p_{\mathrm{f}} = 2,3$ using the sub-domain residual estimator for $ka = 1,\ldots,15$

ka	$p_{\mathrm{f}} = 2$	$p_{\mathrm{f}} = 3$	ka	$p_{\mathrm{f}} = 2$	$p_{\mathrm{f}} = 3$
1	0.6924	0.3946	9	1.4693	0.8138
2	0.5990	0.6848	10	0.9220	1.0748
3	0.6846	0.4926	*11*	*0.1131*	*0.0696*
4	0.9740	1.1176	12	1.0447	0.7675
5	1.7748	1.2492	13	2.7795	0.7610
6	1.7382	1.0288	*14*	*0.6469*	*0.1181*
7	1.2310	0.6539	15	2.2464	0.7834
8	*0.9351*	*0.2195*			

Here we used $p'_{\mathrm{s}} = p_{\mathrm{s}} + 2$, and $p'_{\mathrm{f}} = p_{\mathrm{f}} + 2$. The numbers given in italics indicate the effectivity indices near the resonant frequencies.

Table 5
Effectivity indices of the estimated error in the radial displacement in L^2-norm of ($\eta^{\mathrm{SDR}}_{u_r,L^2(\Omega_{\mathrm{f}})}$) for $p_{\mathrm{s}} = p_{\mathrm{f}} = 2,3$ using the sub-domain residual estimator for $ka = 1,\ldots,15$

ka	$p_{\mathrm{s}} = 2$	$p_{\mathrm{s}} = 3$	ka	$p_{\mathrm{s}} = 2$	$p_{\mathrm{s}} = 3$
1	1.0352	1.6593	9	0.4852	0.3191
2	1.0246	1.6493	10	0.3527	0.2341
3	1.0012	1.6226	*11*	*0.0308*	*0.0103*
4	0.9107	1.1214	12	0.1126	0.1225
5	0.9626	0.5435	13	0.2909	0.1194
6	0.9348	0.6421	*14*	*0.0469*	*0.0153*
7	0.7570	0.3314	15	0.1755	0.2583
8	*0.2424*	*0.0927*			

Here we used $p'_{\mathrm{s}} = p_{\mathrm{s}} + 2$, and $p'_{\mathrm{f}} = p_{\mathrm{f}} + 2$. The numbers given in italics indicate the effectivity indices near the resonant frequencies.

Remark 2. Note that here we did not present the results for $p_f = 1$, or $p_s = 1$. It is well known that for this kind of problem, with low-order finite element approximation, the pollution error is the dominant one (see [6,5] and the references therein). The local error indicators do not capture the pollution error and hence have low effectivity indices. For example, in the example problem considered here, we found that the effectivity indices of the sub-domain residual estimator is around 0.2. However the effectivity indices of the global residual estimator, which is based on the solution of the global residual equation and hence captures both the local and the pollution error, has very good effectivity indices of around 0.95. There are various ways to estimate the pollution error (see [6]) which are beyond the scope of this discussion.

5. Conclusion and future work

We have a demonstrated the advantages of using *p*-refinement, in terms of exponential error convergence, for a class of structural-acoustics problems.

We have also presented a practical and computationally effective recipe for sub-domain-based error estimation for the structural-acoustics problems in 3D. Our presented method relies on using a Dirichlet sub-domain variational-form thus obviating the complexity, especially for unstructured mesh in three space dimensions, of flux-balancing needed in the Neumann type formulations. Although not presented in this paper, the sub-domain residual estimator can be used effectively to estimate the error in quantities of interest by estimating the error in the primal and the dual solution (see [9] for details of error estimation in the quantity of interest).

Additionally, the next steps in error control involve using the estimated error to adapt the approximation by adjusting the interpolation degrees in a spatially varying manner. Our *p*-approximation strategy [13,14] is tied to individual mesh topological entities and not just to elements in the approximation. This makes for greater flexibility and finer control of refinement. Also, for more general problems where the solution may have discontinuities or localized high gradients, a combination of *h*- and *p*-adaptation is more suitable.

Acknowledgments

The research reported in this paper was funded by NASA and a CHSSI award from the HPCMPO. Their support is gratefully acknowledged.

References

[1] F. Ihlenburg, Finite Element Analysis of Acoustic Scattering, Springer-Verlag, New York, 1998.
[2] P.J. Roache, Verification and Validation in Computational Science and Engineering, Hermosa Publishers, Albuquerque NM, 1998.
[3] R. Ohayon, C. Soize, Structural Acoustics and Vibration, Academic Press, San Diego, CA, 1998.
[4] S. Dey, J.J. Shirron, L.S. Couchman, Mid-frequency structural acoustic and vibration analysis in arbitrary, curved, three-dimensional domains, Comput. Struct. 79 (2001) 617–629.
[5] N.N. Abboud, P.M. Pinsky, Finite element dispersion analysis for the three-dimensional second-order scalar wave equation, Int. J. Numer. Methods Engrg. 35 (1992) 1183–1218.
[6] F. Ihlenburg, I. Babuska, Dispersion analysis and error estimation of Galerkin finite element methods for the numerical computation of waves, Int. J. Numer. Methods Engrg. 38 (1995) 3745–3774.
[7] S. Dey, Evaluation of *p*-FEM approximations for mid-frequency elasto-acoustics, J. Comput. Acoust. 11 (2003) 195–225.
[8] C.W.S. To, Application of finite element method for evaluation of velocity response of anvils, J. Sound Vib. 84 (1982) 529–548.

[9] M. Ainsworth, J.T. Oden, A-posteriori Error Estimation in Finite Element Analysis, John Wiley, New York, 2000.
[10] I. Babuska, W.C. Rheinboldt, A-posteriori error estimates for the finite element method, Int. J. Numer. Methods Engrg. 12 (1978) 1597–1615.
[11] P. Morin, R.H. Nochetto, K.G. Siebert, Local problems on stars: a-posteriori error estimators, convergence, and performance, Math. Comput. 72 (2003) 1067–1097.
[12] D.K. Datta, Computer analysis of error estimation in finite element computations for elliptic and parabolic problems, Ph.D. dissertation, Texas A&M University, 2001.
[13] S. Dey, Geometry-based three-dimensional *hp*-finite element modeling and computations, Ph.D. dissertation, Rensselaer Polytechnic Institute, Troy, NY, 1997.
[14] M.S. Shephard, S. Dey, J.E. Flaherty, A straightforward structure to construct shape functions for variable *p*-order meshes, Comput. Methods Appl. Mech. Engrg. 147 (1997) 209–223.